Available online at www.sciencedirect.com
ScienceDirect
Applied Geochemistry 22 (2007) 2735–2757
Applied Geochemistry
www.elsevier.com/locate/apgeochem

Characterization of the reactivity of riverine heterogeneous sediments using a facies-based approach; the Rhine–Meuse delta (The Netherlands)

Pieter-Jan van Helvoort [a,*], Jasper Griffioen [b], Niels Hartog [c]

[a] *Department of Environmental Technology, Wageningen University and Research Centre Bomenweg 2, Biotechnion Building no. 307, 6703 HD Wageningen, The Netherlands*
[b] *TNO Geological Survey of The Netherlands, Princetonlaan 6, 3584 CB Utrecht, The Netherlands*
[c] *Department of Earth Sciences, University of Waterloo, Waterloo, ON, Canada N2L 3G1*

Received 16 November 2006; accepted 8 June 2007
Editorial handling by R. Fuge
Available online 14 August 2007

Abstract

Large groundwater resources are found in densely populated lowland areas, which consist often of young unconsolidated and reduced sediments. When anthropogenic activities lead to oxygenation of the aquifer, breakdown of the main reduced fractions, i.e. sedimentary organic matter (SOM) and pyrite, could lead to severe groundwater deterioration such as acidification, heavy metal mobilization, and increased hardness. The characterization of the reactive properties of these sediments is important in predicting groundwater deterioration, but is often complicated by the high degree of heterogeneity of these sediments. In this study, the potential reduction capacity (PRC, based on SOM and pyrite content), the potential buffer capacity (PBC, based on carbonate content), potential acidification capacity (PAC, based on the potential acid production by sulfide oxidation), and the measured reduction capacity (MRC) of five facies, which are typical of the riverine sediments in the Rhine–Meuse delta (The Netherlands) were determined. A universal facies-classification model was used to classify the deposits into more homogeneous sub-units based on lithologic and geogenic properties, with a further sub-division into oxic or anoxic redox environment based upon groundwater data and field observations. The bulk chemical data show strong variation across facies for the median values of PRC (186–9093 mmol O_2 kg^{-1}), PBC (17–132 mmol O_2 kg^{-1}), and PAC (36–1530 mmol H^+ kg^{-1}). The MRC was measured as reactivity to molecular O_2 exposure and was 0.5–567.3 mmol O_2 kg^{-1}. Steady-state oxidation rates were in the wide range of 0.001–10.355 mmol O_2 kg^{-1} day^{-1} but were typically about 3–8 times faster in fine facies than in coarse facies. Both the PRC and MRC depend strongly on grain size, but also on the syn/post-depositional environment and redox conditions. The main part of the PRC consists of SOM, but pyrite reactivity is higher than SOM reactivity as shown by the relative depletion of pyrite in oxic subfacies and the preferential oxidation during the oxidation experiments. Some facies are very prone to acidification because the PAC is higher than the PBC, but the oxidation experiments also show that acidification could already start before the PRC is fully exhausted. This study, is one of the few that combines bulk chemical data,

* Corresponding author. Present address: Zeemanlaan 166, 3572 ZH Utrecht, The Netherlands. Fax: +31 30 2564 755.
E-mail addresses: helvoort@gmail.com, pieter-jan.vanhelvoort@wur.nl (P.-J. van Helvoort).

0883-2927/$ - see front matter
doi:10.1016/j.apgeochem.2007.06.016

groundwater data, and reactivity measurements and shows that a facies-based approach is a practical tool in characterizing the reactivity of heterogeneous deposits.

1. Introduction

Many of the world's important groundwater resources exist in unconsolidated sediments often found in densely populated lowlands (Morris et al., 2003). Anthropogenic activities introduce vast amounts of oxidants into these naturally reduced sediments, and NO_3^- is probably one of the best known oxidants entering groundwater systems all over the world (Engesgaard and Kipp, 1992; Kölle et al., 1985; Korom, 1992; Postma et al., 1991; van Beek, 2000; van Beek et al., 1988). In addition, artificially recharged surface waters (Bierens de Haan et al., 1994; Stuyfzand et al., 1997) and river bank filtrates (Bourg and Bertin, 1993; Doussan et al., 1997; Massmann et al., 2004; Stuyfzand, 1989; von Gunten et al., 1991) also introduce oxic recharge to aquifers. Artificial lowering of the groundwater tables in well fields or lowland polder areas exposes the subsurface directly to air, leading to oxidation of the anoxic subsurface (Bierens de Haan et al., 1994; Kinniburgh et al., 1994; Massmann et al., 2003; Ritsema and Groenenberg, 1993). The oxidation of aquifer material triggers a wide range of secondary processes potentially leading to groundwater deterioration, like the oxidation of Fe sulfides that causes acidification and heavy metal release (Gäbler, 1997; Larsen and Postma, 1997; Mol, 2002; Santos et al., 2002; Schipper et al., 2000; van Helvoort et al., 2000), or increased hardness due to enhanced carbonate dissolution. As these reactive fractions have a large imprint on groundwater quality, it is important to know their extent (amount) and efficiency (reactivity).

The total reduction capacity of unconsolidated aquifer material, sometimes referred to as TRC (Hartog et al., 2002; Heron and Christensen, 1994, 1995), are sedimentary organic matter (SOM) and pyrite (Christensen et al., 2000; Hartog et al., 2002, 2004; Heron and Christensen, 1995; Postma et al., 1991), although small amounts of other reductants like siderite ($FeCO_3$) or vivianite ($Fe_3(PO_4)_2 \cdot 8H_2O$) may also be present (Hartog et al., 2002; Stuyfzand et al., 1997). The main acid buffering capacity of the aquifer sediments is the carbonate fraction. The characterization of these reactive properties is thus highly important in predicting groundwater deterioration, but is often complicated by the high degree of heterogeneity of these sediments. As a result, variation in reactive properties is often observed (Allen-King et al., 1998; Barber et al., 1992; Christiansen et al., 1998; Davis et al., 1993; Hashagen et al., 1998; Kelly, 1997; MacIntyre et al., 1998; van Helvoort, 2003; Zhu and Burden, 2001). Some workers have used a facies-based approach while determining reactive properties. For example, Allen-King et al. (1998) determined sorption properties of dichloro-ethane after classifying aquifer deposits into sedimentary facies using grain size and lithogenesis. van Helvoort (2003) followed a similar method for a bulk chemical characterization of heterogeneous riverine sediments in the Rhine–Meuse delta (The Netherlands). Using the facies concept, it seems possible to classify heterogeneous deposits into more or less homogeneous sediment.

In this study, a facies-based approach was applied to characterize the reactive properties of heterogeneous fluvio-eolian deposits found in the Rhine–Meuse deltaic plain (The Netherlands). The specific goals were (1) to characterize the potential reduction capacity (PRC), the potential buffer capacity (PBC), the potential acidification capacity (PAC), and (2) to measure the actual reactivity of these reactive fractions to molecular O_2 and H^+. The PRC, PBC and PAC were calculated from bulk chemical analyses of 132 sediment samples. A selection of 20 samples was exposed to molecular O_2 to determine reactivity in terms of measured reduction capacity (MRC) and measured buffer capacity (MBC). The reactivity data were also used to estimate overall oxidation rates. A universal facies classification system (Miall, 1985, 1996) was used to classify these deposits into facies units, which occasionally were sub-divided into oxic and anoxic subvariants. All samples were classified into one of these facies, according to lithology, grain size and redox environment (as derived from groundwater data).

2. Material and methods

2.1. Site description

2.1.1. Geology

The Bommelerwaard field site is located in the Rhine–Meuse deltaic plain (The Netherlands), with the rivers Rhine and Meuse just to the north and south, respectively (Fig. 1a). Much of the deltaic plain was formed by backfilling of the palaeo Rhine–Meuse river valley due to a rapid rise of the mean sea level during the Early Holocene (van de Plassche, 1980, 1981; van Dijk et al., 1991). Except for the eolian dune deposits, which were formed by re-deposition of wind-blown river bed material during the Late Pleistocene, all other deposits are of Holocene age and fluvial origin. The sandy Holocene channel deposits were meandering precursors of the current Rhine and Meuse rivers (Berendsen, 1998; Berendsen et al., 1995; Berendsen and Stouthamer, 2001; Stouthamer and Berendsen, 2000; Törnqvist, 1993, 1994; Weerts, 1996; Weerts and Berendsen, 1995), and are often lined by silty levee deposits, and

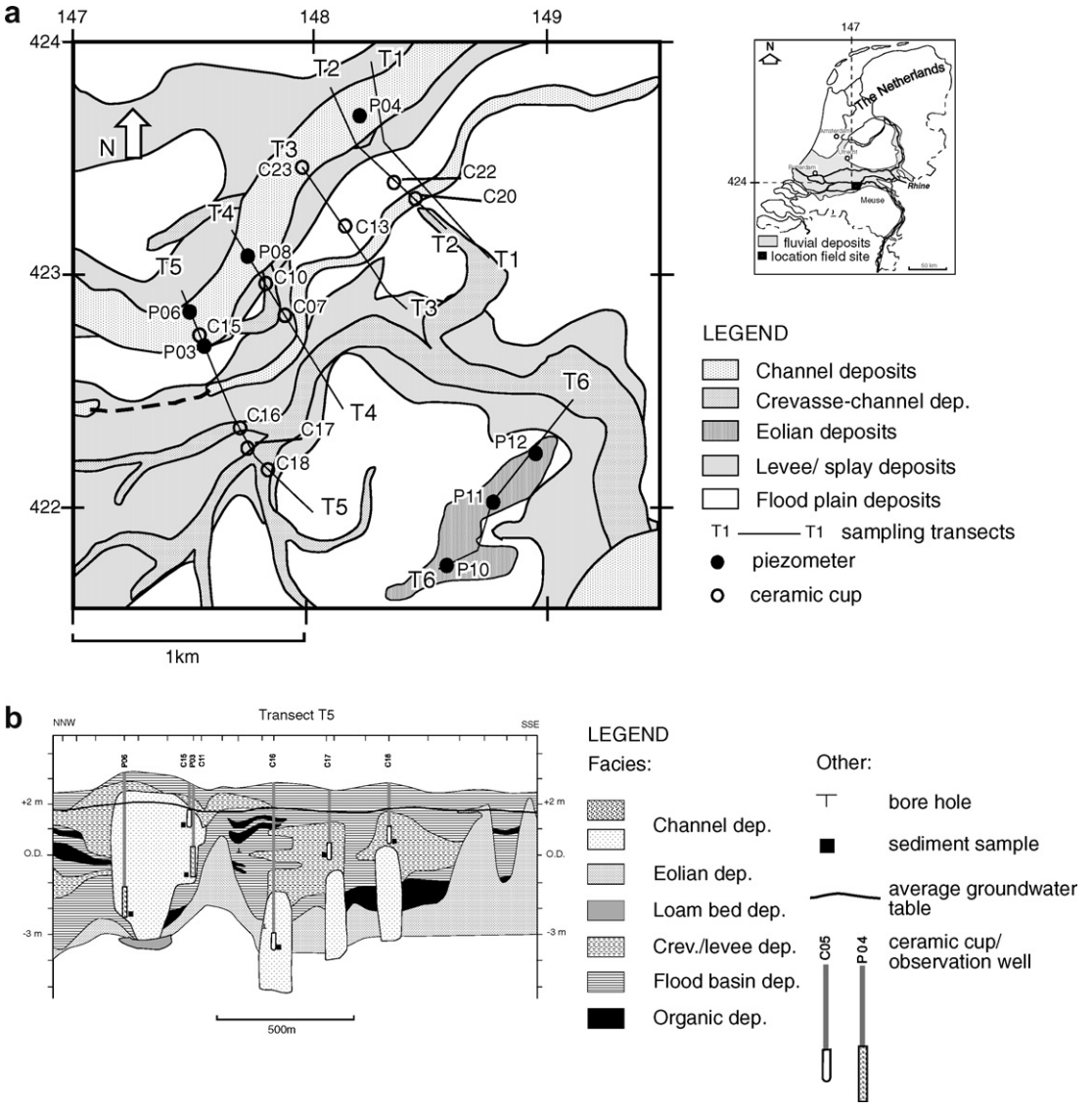

Fig. 1. (a) location of study area in the Dutch fluvial district, local facies distribution, and sampling locations, and (b) cross-section along transect T5 showing the facies distributions in the subsurface. The transect was drawn using accessory data from about 50 bore holes, which, for simplicity, have not been drawn on the map.

occasionally crevasse-splays. The flood plains are characterized by extensive clay deposits and organic deposits (originally peat bogs). The fluvio-eolian deposits typically have a high degree of heterogeneity, as a result of multiple displacements of the meandering channels combined with fast sedimentation rates (Stouthamer and Berendsen, 2000; Törnqvist, 1994). In the study area, these deposits are 3–8 m thick and lay on top of Pleistocene sands and gravels deposited by peri-glacial braided rivers (cross-section in Fig. 1b). Following Weerts (1996) as the main study on local facies lithology, the fluvio-eolian deposits were divided into five lithofacies: channel deposits, crevasse-levee deposits, eolian dune deposits, flood basin deposits and organic deposits. The facies division was made according to depositional environment, textural and structural properties (Table 1), following the concept of architectural element analysis introduced by Miall (1985). Field observations on sediment colour and groundwater level were used to subdivide the facies further into oxic or anoxic redox environments, and the eolian dune deposits were subdivided into calcareous and non-calcareous based on visible reaction with HCl in the field.

2.1.2. Geohydrology

The fluvio-eolian deposits form a semi-confining layer covering a major aquifer of Pleistocene sands and gravels, which is present in large parts of the delta area. The confining parts consist of flood basin deposits, and the unconfining parts consist of permeable Holocene channels deposits, which connect to the underlying Pleistocene aquifer.

Like in many polder areas in The Netherlands, the hydrological situation in the Bommelerwaard is complex due to large variations of hydraulic conductivity, the presence of two large rivers, an extensive surface drainage network, land subsidence due to excessive drainage, and the presence of groundwater abstraction wells. These factors all have altered the original hydraulic gradients in both the semi-confining layer as well as in the underlying Pleistocene aquifer. Although the rivers Rhine and Meuse are nett infiltrating on a yearly basis, there is a complex transient hydraulic system with vertical flow reversals (infiltration vs. upward seepage) and horizontal flow reversals (river bank infiltration vs. ex-filtration) over short distances (10–100 s of meters) or time frames (seasonal).

2.2. Sampling and analyses

A set of 132 sediment samples was collected from the five main facies, including 20 samples for incubation experiments. The reactivity samples were taken from bore holes using a hand-corer and stainless steel sampling tubes 4 cm in diameter and 20 cm long. The tubes were sealed and directly stored at 4 °C in a pres-

Table 1
Facies descriptions and sub facies divisions

Facies	Lithology	Sub facies	Description
Channel deposits	Very fine to coarse sand (105–2000 μm), fine sand and silty clay layers on accretion surface, fining upward	ChanOX	Aerobic facies, unconfined[a]
		ChanRE	Anaerobic facies, unconfined[b]
Crevasse splay/natural levee deposits	Levees: horizontally laminated sandy–silty clay, small lenses of (very) fine sand (105–210 μm)	CrlvOX	Aerobic facies[a]
	Splays: horizontally laminated and crossbedded sandy–silty clay, lenses of very fine to fine sand (105–210 μm)	CrlvRE	Anearobic facies[b]
Eolian deposits	Very fine to fine sand (105–210 μm), structureless	DuneRE	Anaerobic non-calcareous facies[c]
		DuneREca	Anaerobic calcareous facies[d]
Flood basin deposits	Massive to very thin laminated clay and humic clay	FlbasOX	Aerobic facies[a]
		FlbasRE	Anearobic facies[b]
Organic deposits	Peat	OrgRE	Anearobic facies[b]

The sediment samples were classified into a facies based on lithology.
[a] Aerobic facies were defined if ambient porewaters or groundwaters had $[Fe^{2+}] \leqslant 5.0$ μmol/L.
[b] Anaerobic facies were defined if ambient porewaters or groundwaters had $[Fe^{2+}] > 5.0$ μmol/L.
[c] Non-calcereous Dune facies has a carbonate content < 0.10 wt%.
[d] Calcereous Dune facies has a carbonate content > 0.10 wt%.

sure vessel under a N_2-atmosphere to prevent oxidation. After sampling, an observation well was installed in a sandy facies or a suction cup in a clayey facies. The other samples were collected from bore holes without conservation precautions or well installation.

In the laboratory, the reactivity samples were opened in a glove box (Braun Labmaster 130) while maintaining molecular O_2 levels below 1 ppm. They were split lengthwise several times to produce subsamples for chemical characterization (see below), moisture content determination, and incubation experiments. For incubation, 25 g of finely grained sediment or 75 g of coarsely grained sediment were weighed, because the highest reactivities were expected for the finely grained deposits. Glass bottles (100 mL, DURAN) were used and stored in pressure vessels under a N_2-atmosphere at 4 °C until incubation.

The complete set of 132 samples was used for bulk chemical analysis. The samples were dried at 70 °C and mechanically ground (Herzog HSM apparatus). X-ray fluorescence (XRF) was used for major element oxide (Al_2O_3, CaO, Fe_2O_3, K_2O, MgO, MnO, Na_2O, P_2O_5, SiO_2 and Ti_2O), and trace element (As, Ba, Bi, Cd, Ce, Cr, Cs, Cu, Ga, La, Mo, Nb, Ni, Pb, Rb, S, Sb, Sn, Sr, Th, U, V, Y, Zn and Zr) determinations. Loss on ignition (LOI) was determined at 950 °C. Sedimentary organic matter and carbonate contents were determined by thermal gravimetric analysis (TGA), using a LECO TGA 608 apparatus. Additional elemental C and S analyses were performed by combustion and infra-red gas-detection (LECO SC) to have duplicates for carbonate-C and SOM-C as derived from TGA, and S analysis determined by XRF respectively.

For total cation exchange capacity (CEC) determination, a standard buffered salt method (Hesse, 1971) was applied to unground subsamples using first Na-acetate to saturate with Na (3 times) and subsequently NH_4-acetate to displace exchangeable Na (also 3 times) while buffering at pH 7 (close to the field pore water pH). The analyses of replicates and ISE standards showed that the precision and accuracy was within 5%. The NH_4-acetate extracts were analyzed for exchangeable Na by ICP-AES (Spectroflame apparatus, SPECTRO analytical instruments).

The wells and suction cups were used for ground water sampling. A total of 167 clear groundwater samples were collected in six sampling campaigns within a 1-year period, leading to 3–6 samples per location. The wells were sampled after pH, electrical conductivity (EC), O_2-saturation and temperature had stabilized as monitored in a flow-through cell. The samples were filtered through a 0.40 μm pore size filter and stored in a sealed 60 mL syringe at 4 °C. Water samples from the ceramic cups were drawn directly into a syringe, sealed and stored at 4 °C. Since the ceramic cup acted as a filter itself, the samples were not filtered again. All water samples were analyzed for alkalinity in the field, using a Merck field titration set. The samples were analyzed within 48 h for Al, Ca, Cd, Cu, Fe, K, Mg, Na, Mn, Pb, S, Si, Zn (ICP-AES, Spectroflame apparatus, SPECTRO analytical instruments), Cl, NH_4, NO_3, PO_4 (auto-analyzer and photometry, SKALAR), alkalinity (acid titration), TIC (TC, TN Analyzer, SKALAR), EC, and pH (Sentron electrodes). The charge balance of the water analyses was within 5%.

2.3. Sediment incubations

The reactivity samples were subjected to the incubation experiment. The batches were prepared by adding about 50 g N_2-purged distilled water to the bottles with sediment and two blanks were also prepared from distilled water. The batches and blanks were kept in the dark at 12 °C while shaking at 100 rpm. After 24 h of sediment-water equilibration, the batches were connected to a respirometer (Micro-Oxymax, Columbus Instruments). For a period of 49 days, the consumption of O_2 and the production of CO_2 were measured by infra-red spectroscopy every 3 h, refilling the headspace with fresh air after each measurement. During the last 14 days of the incubation, the batches were shaken at 200 rpm to see whether intensified homogenization of the suspension had influence on reaction rates. After incubation, the batches were centrifuged and the supernatants were analyzed for the same components and in the same way as the groundwater samples (see Section 2.2).

2.4. Data analysis

2.4.1. Bulk chemical analyses

The bulk chemical data were used to calculate median values of PRC, PBC and PAC for each facies. The PRC is defined here as the sum of potential reduction capacities of SOM and pyrite and is expressed in mmol O_2 kg^{-1} dry sediment similar to the TRC defined by Hartog et al. (2002):

$$TRC = PRC_{tot} = PRC_{SOM} + PRC_{Pyrite} = 1[TOC] + 3\frac{3}{4}[FeS_2] \quad (1)$$

where [TOC] and [FeS_2] are the amounts of total organic C and pyrite in mmol/kg dry sediment respectively. PRC is introduced as a new term to accentuate the difference between *potential* and *measured* reduction capacities. The coefficients in Eq. (1) are derived from stoichiometric oxidation reactions of SOM and pyrite with O_2 (Table 2, reactions R1a, R1b and R2), assuming CH_2O to be the model compound for SOM (e.g. Christensen et al., 2000). The amounts of TOC and pyrite were derived from the bulk chemical analyses of SOM and S content, respectively.

The PBC (expressed in mmol H^+ kg^{-1} dry sediment) is defined as the amount of $CaCO_3$ present in the sediment, assuming that carbonate is the foremost acid neutralizing component and neutralizes H^+ on a one to one mole ratio according to carbonate dissolution:

$$CaCO_3 + H^+ \rightarrow Ca^{2+} + HCO_3^-$$

leading to:

$$PBC = 1[CaCO_3] \quad (2)$$

with [$CaCO_3$] the amount of carbonate in mmol kg^{-1} dry sediment. In addition to the PBC, the potential acidification capacity (PAC) is also defined as the amount of H^+ (in mmol kg^{-1} dry sediment) potentially produced by complete pyrite oxidation (reaction R1b, Table 2):

$$PAC = 4[FeS_2] \quad (3)$$

When the PAC exceeds the PBC, the amount of acid produced upon complete pyrite oxidation (reactions R1a and R1b, Table 2) can not be neutralized by the carbonates present and thus there is a high potential of acidification.

2.4.2. Sediment incubations

Two main types of data are generated from the sediment incubation experiments: (1) O_2 and CO_2 respiration data, and (2) the supernatant compositions. The respiration data were used to determine reactivity in terms of total amount of O_2 consumption (after substraction of the amount of O_2 consumed to reach atmospheric saturation in the supernatant, being 0.26 mmol O_2 L^{-1} at 12 °C). This is defined as MRC_{tot} (expressed in mmol O_2 kg^{-1} dry sediment). Analogous to PRC_{tot}, the individual shares for SOM and pyrite in the MRC_{tot} can be defined:

$$MRC_{tot} = \text{total amount of } O_2 \text{ consumed} = MRC_{SOM} + MRC_{Pyrite} \quad (4)$$

The supernatant composition afterwards was used to estimate the shares of MRC_{SOM} and MRC_{Pyrite} per incubation (see next paragraph). The dominant oxidation reactions were also inferred by comparing the (theoretical) diagnostic CO_2/O_2 ratios (Table 2) with the slopes of CO_2 production vs. O_2 consumption during steady state (Hartog et al., 2002). The time series of O_2 consumption were used to derive the oxidation rates (in mmol O_2 kg^{-1} d^{-1}) by calculating the derivative of the O_2 consumption vs. time curves for each 3 h step.

The supernatant compositions were used to determine pyrite oxidation and carbonate dissolution quantitatively using the index parameters [SO_4] and [Ca] + [Mg], respectively (index parameters are in the last column of Table 2). The MRC_{Pyrite} was calculated converting the amount of SO_4^{2-} in the supernatants to O_2 equivalents using the stoichiometric coefficients for O_2 and SO_4^{2-} in reaction R1a from Table 2. Note that the MRC_{SOM} could not be calculated directly, because there are no suitable index parameters in the supernatant,

Table 2
Oxidation reactions of pyrite (FeS_2) and SOM (CH_2O) with O_2

Reaction		Process	CO_2/O_2	CO_2[a]$/O_2$	Index parameters
R1a.	$FeS_2 + 3\frac{3}{4}O_2 + 3\frac{1}{2}H_2O \rightarrow Fe(OH)_3 + 2SO_4^{2-}$	Un-buffered pyrite oxidation	0	0	$[SO_4^{2-}]$, acidic pH
R1b.	$FeS_2 + 3\frac{3}{4}O_2 + 1\frac{1}{2}H_2O + 2CaCO_3 \rightarrow Fe(OH)_3 + 2Ca^{2+} + 2SO_4^{2-} + 2CO_2$	Buffered pyrite oxidation	8/15	8/15	[b]$[Ca^{2+}]/[SO_4^{2-}] = 1$
R2.	$CH_2O + O_2 \rightarrow CO_2 + H_2O$	SOM oxidation	1	1	TIC or pCO_2
R3.	$CO_2 + CaCO_3 \rightarrow Ca^{2+} + 2HCO_3^-$	Carbonate buffering	0	2	[b]$[Ca^{2+}]$/alkalinity = 0.5

[a] CO_2^* = corrected for alkalinity storage effect.
[b] $[Ca^{2+}] = [Ca^{2+}] + [Mg^{2+}]$; Carbonates were found to have a considerable amount of Mg (see text).

nor is the CO_2 production indicative of SOM oxidation alone, as CO_2 was also produced by carbonate dissolution. Therefore, the MRC_{SOM} was calculated by difference between MRC_{tot} and MRC_{Pyrite} (expression 4). The MBC was determined by converting the [Ca] + [Mg] in the supernatant to the amount of carbonate dissolved from the sediment and accounting for calcite dissolution at the ambient CO_2 pressure. Magnesium was included because the Ca/Mg-carbonates in these fluvio-eaolian deposits have 9.2 wt% of $MgCO_3$, as quantified from bulk chemistry of calcareous sand samples that were poor in accessory Mg-bearing components like micas and clay minerals. The MBC is, like the PBC, expressed in mmol H^+ kg^{-1} dry sediment.

The hydrochemical computer program PHREEQC 2.1 (Parkhurst and Appelo, 1999) was used to calculate alkalinity and CO_2 pressure in the supernatant using the measured TIC and pH. Also, the saturation indices (SI's) for calcite, gypsum and jarosite were calculated to determine whether mineral precipitation could have affected the concentrations of one of the index parameters Ca, Mg and SO_4.

3. Results

3.1. Sediment geochemistry

The median Al_2O_3, pyrite, SOM and carbonate contents per facies are given in Table 3, where Table 4 lists the individual characteristics of the incubated samples. The Al_2O_3 content increases with decreasing grain size as a result of increasing clay mineral content (Huisman and Kiden, 1998). The values listed in Table 3 are consistent with the textural descriptions of Table 2, placing the facies order of decreasing grain size: channel deposits ~ eolian dune deposits > crevasse–levee deposits > organic deposits > flood basin deposits. The Al_2O_3 content in the organic deposits (OrgRE facies) is very low because of substantial dilution of the textural matrix by the high organic matter content.

Carbonate contents vary substantially over the facies, with the highest median in crevasse-levee facies (10.66–11.32 wt%) and the lowest in the DuneRE facies (0.17 wt%). Carbonate fragments were enriched in the crevasse-levee facies by hydrodynamic sorting during deposition (van Helvoort et al., 2005), resulting in extreme carbonate contents. The DuneRE are depleted of carbonates, because they have been leached by infiltrating

Table 3
Median values of bulk chemistry and reactive parameters per facies (data from 132 sediment samples)

Facies	*N*	Al_2O_3 (wt%)	Fe_2O_3 (wt%)	Pyrite (wt%)	SOM (wt%)	Carbonate (wt%)	CEC (meq/100 g)	PRC_{som} (mmol O_2/kg)	PRC_{pyr} (mmol O_2/kg)	[a]Ratio (–)	PRC_{tot} (mmol O_2/kg)	PBC (mmol H^+/kg)	PAC (mmol H^+/kg)
ChanOX	17	3.47	0.79	0.05	0.52	1.53	1.30	209	18	11.6	211	153	36
ChanRE	26	3.88	0.84	0.08	0.50	1.70	1.10	198	26	7.6	209	170	52
CrlvOX	8	9.40	3.33	0.04	3.08	10.66	16.68	1232	12	102.7	1258	1066	24
CrlvRE	15	10.02	4.06	0.27	4.60	11.32	15.93	1842	88	20.9	1894	1132	186
DuneRE	12	2.14	0.38	0.11	0.34	0.17	1.00	134	35	3.8	186	17	70
DuneREca	4	5.22	1.64	0.48	4.91	2.01	11.20	1965	158	12.4	2071	201	316
FlbasOX	9	14.77	6.74	0.05	5.24	4.99	41.78	2096	18	116.4	2108	499	36
FlbasRE	21	15.90	6.19	0.39	6.67	2.09	33.43	2666	129	20.7	2771	209	258
OrgRE	20	12.19	6.02	2.34	21.09	2.39	52.25	8436	765	11.0	9093	239	1530

[a] Ratio of PRCsom/PRCpyr.

Table 4
Bulk chemistry and reactive parameters of the 20 incubated samples

Sample	Facies	Al_2O_3 (wt%)	Fe_2O_3 (wt%)	Pyrite (wt%)	SOM (wt%)	Carbonate (wt%)	CEC (meq/100 g)	PRC_{som} (mmol O_2/kg)	PRC_{pyr} (mmol O_2/kg)	[a]Ratio (–)	PRC_{tot} (mmol O_2/kg)	PBC (mmol H^+/kg)	PAC (mmol H^+/kg)
C15	ChanOX	6.31	1.25	0.05	0.78	11.27	1.96	241	18	17.3	259	1147	35
C23	ChanOX	4.54	0.93	0.07	0.42	2.33	1.28	120	23	7.3	143	262	47
P03	ChanRE	5.72	1.06	0.07	0.70	5.66	2.07	209	70	12.2	279	663	47
P04	ChanRE	4.03	0.90	0.13	0.62	6.38	1.19	187	23	6.0	210	504	82
P06	ChanRE	3.47	0.69	0.23	0.71	4.85	1.70	234	41	3.8	275	153	152
P08	ChanRE	5.28	0.94	0.13	0.70	1.24	1.31	231	76	6.9	308	523	82
C01	ChanRE	5.42	1.13	0.21	0.57	0.23	1.90	125	41	3.3	166	608	141
C10	CrlvOX	8.88	3.23	0.11	2.85	14.82	15.62	961	35	32.6	996	1481	70
C16	CrlvRE	7.20	2.79	0.25	4.13	16.51	7.15	1400	82	20.1	1483	1666	164
C17	CrlvRE	8.64	4.59	0.16	2.47	0.94	13.30	880	53	18.7	933	94	105
C18	CrlvRE	8.54	3.15	0.09	2.19	17.77	10.15	741	29	30.2	770	1787	59
C20	CrlvRE	7.37	2.56	0.21	2.45	16.03	11.44	834	70	14.0	905	1624	141
P10	DuneRE	2.38	0.38	0.20	0.29	0.20	1.00	125	64	1.8	189	20	129
P11	DuneRE	2.07	0.31	0.05	0.17	0.14	0.78	74	18	3.7	92	14	35
P12	DuneREca	5.66	1.89	0.47	3.41	5.89	10.67	1203	152	9.0	1355	626	305
C05	FlbasRE	15.04	6.71	0.39	6.47	2.57	26.88	2211	129	20.1	2339	263	258
C07	FlbasRE	18.83	6.82	0.56	9.58	2.46	42.65	3329	182	21.0	3510	201	363
C09	FlbasRE	6.93	2.47	0.29	3.50	0.96	31.62	1220	94	14.9	1314	88	188
C13	OrgRE	10.76	6.24	5.84	44.23	3.54	83.20	16670	1911	9.3	18580	208	3822
C22	OrgRE	10.68	7.17	4.82	37.91	4.15	80.59	14103	1577	9.6	15680	215	3154

Pyrite content was calculated from XRF sulfur analysis.
[a] Ratio of PRCsom/PRCpyr.

rainwater during the Late Pleistocene and Early Holocene before burial by Holocene fluvial deposits. The larger part of the eolian dunes belong to the DuneRE subfacies, but the DuneREca subfacies is typically found at the bases of dunes (near the Pleistocene substratum), where decalcification did not occur because infiltrating water was already calcite-saturated. With ongoing groundwater table rise and sedimentary burial throughout the Holocene (Berendsen, 1998; Cohen, 2003; van de Plassche, 1980), carbonate saturated groundwater invaded the higher elevated parts of the dunes and finally stopped decalcification.

The geochemical characteristics of the incubated samples in Table 4 are a good reflection of the median values per facies as reported in Table 3. In general, the individual samples represent the (sub)facies within 1.5 times the median range. Larger deviations from median subfacies composition exist for the carbonate contents of samples from the channel facies.

3.2. Potential reactivity (PRC, PBC, PAC)

The median values of PRC_{SOM}, PRC_{Pyrite}, PRC_{tot}, PBC and PAC are listed in Table 3. The pyrite and SOM contents have much in common showing a clear trend with redox environment and a weaker one with grain size. All anoxic subfacies have higher pyrite and SOM contents than their oxic counterparts, and the amounts of pyrite and SOM tend to increase with decreasing grain size. This reverse trend with grain size is commonly observed in unconsolidated sediments (Berner, 1971). The PRC_{SOM} is considerably larger than PRC_{Pyrite} in all facies, and also increases with decreasing grain size. The sandy facies have lowest PRC_{SOM} (134–209 mmol O_2 kg^{-1}), followed by silty and clayey facies (1232–2666 mmol O_2 kg^{-1}), and then the organic deposits (8436 mmol O_2 kg^{-1}), with the same tendency to be higher in anoxic subfacies. The PRC_{Pyrite} follows a different pattern, which is not entirely dictated by grain size alone. This is illustrated by the high PRC_{Pyrite} in calcareous eolian dune deposits (DuneREca), which consists also of sandy material like the channel deposits, which have lower PRC_{Pyrite}. Like PRC_{SOM}, the PRC_{tot} varies considerably over the facies with the lowest in the sandy facies (186–211 mmol O_2 kg^{-1}), high in the clayey facies (1258–2771 mmol O_2 kg^{-1}), and extreme in the organic deposits (9093 mmol O_2 kg^{-1}). In the crevasse-levee and flood basin deposits, the PRC_{tot} is largest in the anoxic subfacies, but in the channel deposits there is no difference between the oxic and anoxic subfacies. The PRC data of the sandy facies comply well with TRC data of Early to Late Pleistocene fluvial sands in the Netherlands ranging from 93 to 199 mmol O_2 kg^{-1} (Hartog et al., 2002).

The PBC follows by definition the carbonate contents, and are highest in the crevasse-levee deposits (1066–1132 mmol H^+ kg^{-1}) and lowest in the DuneRE facies (17 mmol H^+ kg^{-1}). The potential reactivities of the incubated samples (see Table 4) are mostly within 1.5 times the median ranges for facies and will not be discussed here separately.

3.3. Groundwater composition

Table 5 lists key parameters describing the groundwater chemistry of the samples selected for incubation. All groundwater samples are of the Ca-HCO_3 type and mostly buffered at pH > 7. The samples from oxic subfacies all have [Fe] and [Mn] smaller than 5 μg/L, and may have elevated NO_3 concentrations indicating a clear anthropogenic component. Field observations of the sediment color indicate that Fe and Mn-reducing groundwaters occur in grey-colored anoxic subfacies indeed, but in some cases NO_3-containing groundwaters were found in reduced sediments like in sample P11 (DuneRE facies). The saturation indices indicate close saturation for calcite (SI = −0.46 to +0.76), and under-saturation for gypsum (SI = −3.13 to −1.04). In reduced facies groundwaters are supersaturated for siderite in most cases, whereas under-saturation occurs in oxic sub facies (−2.01 to −1.34). The CO_2 pressure was between $10^{-1.0}$ and $10^{-2.1}$ atm, and is slightly higher in the FlbasRE and OrgRE facies compared to the other facies. The PHREEQC calculations also show that 93–99% of the available exchange sites should be occupied with Ca or Mg.

3.4. Sediment incubation

3.4.1. Measured reactivity and dominant processes

Table 6 summarises the most important results of the respiration experiments. The MRC_{tot} differs considerably among the facies, and indicates a general increase of MRC_{tot} with decreasing grain size. The lowest MRC_{tot} was measured for the sandy samples from the non calcareous eolian dune facies (DuneRE) and the channel facies (ChanOX and

Table 5
Groundwater chemistry at the sampling sites

Sample	Facies	Ca	Cl	Fe	K	Mg	Mn	Na	NH_4	NO_3	SO_4	TIC	pH (–)	EC ($\mu S/cm^2$)	Ca-X_2 charge fraction	Mg-X_2 charge fraction	pCO_2 (atm)	Calcite (SI)	Siderite (SI)	Gypsum (SI)
C15	ChanOX	3.6	1.0	0.3	0.07	0.6	0.7	1.1	0.01	0.22	1.2	6.4	7.7	861	0.89	0.09	−2.0	0.5	−1.3	−1.3
C23	ChanOX	3.3	1.1	<0.1	0.13	0.6	0.0	1.1	<0.01	1.45	0.8	5.8	7.2		0.89	0.10	−1.8	0.2	−2.0	−1.5
C01	ChanRE	3.1	1.4	0.7	0.02	0.5	8.3	1.1	<0.01	<0.01	0.5	6.0	7.4	764	0.89	0.10	−1.8	0.3	−1.1	−1.8
P03	ChanRE	2.3	1.5	39.1	0.10	0.5	8.6	1.6	0.13	<0.01	0.2	6.4	7.9	696	0.86	0.10	−1.8	0.1	0.6	−2.3
P04	ChanRE	4.4	1.1	93.5	0.03	0.6	27.8	0.6	0.04	<0.01	2.1	6.3	7.5	949	0.90	0.08	−1.8	0.3	0.9	−1.0
P06	ChanRE	2.0	1.2	18.7	0.11	0.4	5.2	1.1	0.01	<0.01	0.3	4.7	7.9	576	0.87	0.12	−2.0	0.0	0.3	−2.0
P08	ChanRE	2.9	1.0	39.0	0.10	0.5	24.3	0.9	0.01	<0.01	0.3	7.2	7.7	721	0.88	0.10	−1.7	0.2	0.6	−2.0
C10	CrlvOX	3.6	1.0	<0.1	0.07	0.6	2.9	1.3	0.01	0.02	1.1	6.8	7.7	857	0.89	0.09	−2.2	0.8	−1.5	−1.4
C16	CrlvRE	3.6	2.1	40.3	0.05	0.6	16.5	1.0	0.18	0.01	0.1	8.6	7.4	898	0.89	0.09	−1.5	0.3	0.6	−2.6
C17	CrlvRE	1.8	1.0	44.1	0.01	0.3	10.6	1.2	0.01	0.01	0.3	4.7	7.3	520	0.88	0.09	−1.7	−0.4	0.3	−2.1
C18	CrlvRE	2.5	1.4	37.0	0.01	0.3	12.9	1.2	<0.01	<0.01	0.1	7.0	7.2	766	0.90	0.08	−1.3	−0.3	0.1	−2.4
C20	CrlvRE	2.6	1.5	55.3	0.02	0.4	15.9	1.3	0.05	<0.01	0.1	6.3	7.6	695	0.89	0.09	−1.7	0.1	0.7	−2.4
P10	DuneRE	3.6	1.4	53.0	0.02	0.6	17.0	1.3	0.02	<0.01	1.5	6.3			0.88	0.09	−1.5	0.1	0.5	−1.3
P11	DuneRE	1.6	1.0	2.1	0.11	0.3	0.3	1.0	<0.01	0.13	0.5	3.3	7.8	504	0.87	0.11	−2.1	−0.2	−0.8	−1.9
P12	DuneREca	2.7	1.6	53.1	0.06	0.4	16.3	1.4	0.18	<0.01	0.4	6.3	7.3	749	0.89	0.08	−1.5	−0.1	0.4	−1.9
C05	FlbasRE	2.4	0.8	316.8	0.03	0.4	28.6	0.3	0.48	<0.01	<0.1	7.1	6.9	626	0.85	0.08	−1.4	−0.2	1.2	−3.1
C07	FlbasRE	2.8	1.5	33.6	0.03	0.5	12.9	1.5	<0.01	<0.01	0.6	6.4	7.4	748	0.89	0.09	−1.4	−0.2	0.1	−1.7
C09	FlbasRE	2.8	0.9	165.1	0.02	0.5	37.8	0.4	0.10	<0.01	<0.1	8.3	7.0	660	0.87	0.10	−1.0	−0.5	0.6	−3.1
C13	OrgRE	4.0	1.0	15.6	<0.01	0.6	45.1	0.5	0.01	<0.01	0.1	11.0	7.2	866	0.90	0.08	−1.0	0.0	−0.2	−2.6
C22	OrgRE	3.5	1.0	65.9	<0.01	0.5	42.2	0.7	0.07	<0.01	<0.1	9.1	7.4	778	0.90	0.08	−1.4	0.1	0.7	−2.7

Concentrations in mmol/L, except Fe and Mn in μmol/L. Values for saturation indices, pCO_2 and exchangeable cations calculated with PHREEQC.

Table 6
Respiration data and measured reactivities

Sample (–)	Facies	Process (–)	Depth (m)	O_2 consumption (mmol/kg)	CO_2 production (mmol/kg)	[a]CO_2/O_2 (–)	MRC_{som} (mmol O_2/kg)	MRC_{pyr} (mmol O_2/kg)	MRC_{tot} (mmol O_2/kg)	MBC (mmol H^+/kg)	[b]MRC_{som} (%)	[b]MRC_{pyr} (%)	[b]MRC_{tot} (%)	[c]MBC (%)
C15	ChanOX	SOM	1.67	2.9	3.3	0.6	2.7	0.2	2.9	1.9	0.9	1.1	1.0	0.2
C23	ChanOX	SOM	2.00	0.5	1.5	0.9	0.4	0.1	0.5	1.1	0.2	0.5	0.3	0.4
C01	ChanRE	pyr-buf SOM	1.70	9.0	4.3	0.5	3.4	5.6	9.0	3.6	1.2	8.0	3.1	0.5
P03	ChanRE	pyr-buf	3.18	5.3	2.6	0.5	2.8	2.5	5.3	2.0	1.1	10.8	2.2	0.4
P04	ChanRE	pyr-buf	4.73	5.2	2.1	0.4	3.0	2.2	5.2	2.2	1.1	5.3	1.7	1.4
P06	ChanRE	SOM	4.84	10.1	6.5	0.7	7.6	2.4	10.1	1.9	2.7	3.2	3.1	0.4
P08	ChanRE	pyr-buf SOM	3.99	3.6	2.5	0.5	1.8	1.8	3.6	1.7	0.8	4.5	2.1	0.3
C10	CrlvOX	SOM	1.00	3.1	4.0	0.8	0.7	2.5	3.1	2.9	0.1	7.0	0.3	0.2
C16	CrlvRE	SOM	5.74	43.0	31.3	1.1	36.4	6.6	43.0	5.7	2.2	8.0	2.5	0.3
C17	CrlvRE	SOM pyr-buf pyr-un	2.71	43.5	8.6	0.4	32.5	11.0	43.5	5.2	3.3	20.8	4.1	5.5
C18	CrlvRE	SOM	2.02	11.8	6.0	0.4	5.3	6.5	11.8	4.3	0.6	22.2	1.3	0.2
C20	CrlvRE	SOM	5.01	21.7	16.5	0.7	12.9	8.8	21.7	5.8	1.3	12.6	2.1	0.4
P10	DuneRE	SOM pyr-un	5.02	2.3	0.3	0.4	1.8	0.5	2.3	0.6	1.5	0.8	1.2	3.2
P11	DuneRE	SOM pyr-un	4.52	1.1	0.0	0.3	0.6	0.5	1.1	0.3	0.9	2.9	1.1	2.4
P12	DuneREca	pyr-buf	4.83	21.3	12.5	0.5	16.1	5.2	21.3	4.3	1.2	3.4	1.4	0.7
C05	FlbasRE	pyr-buf pyr-un	4.70	84.1	32.4	0.4	71.9	12.2	84.1	11.6	2.8	9.4	3.2	4.4
C07	FlbasRE	SOM pyr-un	2.80	73.1	9.9	0.2	51.2	21.8	73.1	11.3	1.3	12.0	1.9	5.6
C09	FlbasRE	pyr-buf pyr-un SOM	5.10	82.8	40.6	0.5	61.1	21.7	82.8	13.3	4.4	23.1	5.5	15.1
C13	OrgRE	SOM pyr-buf pyr-un	2.25	955.9	63.9	0.1	388.6	567.3	955.9	232.5	2.2	29.7	4.9	111.6
C22	OrgRE	SOM pyr-buf pyr-un	2.50	393.8	32.1	0.1	114.8	279.1	393.8	134.5	0.8	17.7	2.4	62.6

[a] As median value.
[b] As percentage of PRC_{SOM} and PRC_{Pyrite}, respectively.
[c] As percentage of PBC.

ChanRE: 0.5–10.1 mmol O_2 kg^{-1}), the calcareous dune facies (DuneREca) and silty crevasse-levee facies (CrlvOX and CrlvRE) had intermediate MRC_{tot} (3.1–43.5 mmol O_2 kg^{-1}), the FlbasRE high (73.1–84.1 mmol O_2 kg^{-1}) and the OrgRE facies extremely high (393.8–955.9 mmol O_2 kg^{-1}).

The samples taken from the oxic channel (ChanOX) and crevasse-levee (CrlvOX) subfacies have a lower MRC_{tot} than their anoxic counterparts. Table 6 shows that MRC_{tot} was only a small fraction of the PRC_{tot} (0.3–5.5%), and that the lowest reactivities (0.3–1.2%) were recorded for the ChanOX, CrlvOX and DuneRE subfacies.

As stated in Section 2.4, the MRC_{Pyrite} was calculated from the SO_4 concentration in the supernatant (Table 7), and subsequently MRC_{SOM} by difference from MRC_{tot}. Sulfate could safely be used as the index parameter in most cases because the saturation indices (SI's) indicate subsaturation of SO_4-bearing minerals (gypsum and jarosite), so SO_4 would not have been removed by precipitation. Four supernatants (P10, P11, C07, C13) were supersaturated for jarosite (high Al, Fe, and SO_4), and in one (C13) both gypsum and jarosite were supersaturated. The precipitation of these minerals may have affected the SO_4 concentration in the supernatant leading to underestimation of MRC_{Pyrite} and consequently, overestimation of MRC_{SOM} in these samples.

For the majority of samples, the absolute MRC_{SOM} is greater than MRC_{Pyrite} (Table 6), which means that the oxidation of SOM is the dominant O_2-consuming process in these samples. However, for many incubations the median CO_2/O_2 ratios in Table 6 are <0.5 instead of 1.0, the latter being the theoretical value for SOM oxidation (reaction R2, Table 2). This indicates that both SOM oxidation and pyrite oxidation (buffered or unbuffered) occurred, notably decreasing the median CO_2/O_2 ratio. Fig. 2 shows that the CO_2 production versus O_2 consumption is not constant in time, indicating that both processes occur in varying intensities. Fig. 2 also shows that the CO_2/O_2 ratio was affected by a CO_2 production lag at the beginning of the experiments, because CO_2 was not transferred to the headspace until the supernatant was CO_2 saturated (see Hartog et al., 2005). It is not likely that CO_2 was transferred from the headspace into the supernatant to establish the CO_2 equilibrium, because no CO_2 consumption was measured. Table 6 shows that in many incubations, the relative MRC_{Pyrite} (MRC_{Pyrite} as percentage of PRC_{Pyrite}) exceeds the relative MRC_{SOM} (MRC_{SOM} as percentage of PRC_{Pyrite}). This implies that pyrite has been preferentially oxidized in these sediment samples. In addition, the relative MRC_{Pyrite} was highest in the finely grained facies, being CrlvRE, FlbasRE and OrgRE facies.

3.4.2. Reaction rates

The initial and steady-state (median) reaction rates at 100 rpm and 200 rpm are reported in Table 8, and Fig. 3 shows the reaction rates as the measured O_2 consumption rate vs. time for three selected samples (P08, C09, C18). In all cases, the initial rates, both at the beginning of the experiment and immediately after increasing the stirring rate to 200 rpm, were higher than the steady-state rates with the result that a significant share of MRC_{tot} had been generated before steady-state was reached. The lowest steady-state rates at 100 rpm were measured in the ChanOX, CrlvOX, and DuneRE facies (0.001–0.014 mmol kg^{-1} d^{-1}), and the highest were found for the OrgRE (1.01–1.94 mmol kg^{-1} d^{-1}). The other anoxic subfacies had rates between 0.016 and 0.17 mmol kg^{-1} d^{-1}, with a generally increasing trend with decreasing grain size order (ChanRE-CrlvRE-FlbasRE). At 200 rpm, reaction rates were faster and also show a wider range among and within facies, but it should be noted that a steady-state was not reached in all cases before the end of the experiment. Generally, a factor 4–8 increase was observed in the finely grained facies (CrlvRE, FlbasRE, and OrgRE) and in the sandy facies a factor 1 to 2 (see last column in Table 8).

3.4.3. Carbonate chemistry and MBC

Fig. 4 shows the relation between supernatant chemistry (Table 7) and different carbonate buffering processes that occurred during the incubations. In Fig. 4a, the relation between TIC and [Ca] + [Mg] shows (1) if the supernatant was in close equilibrium with atmospheric conditions (TIC = 1.4 mmol/L, [Ca] + [Mg] = 0.7 mmol/L at CO_2 pressure = $10^{-3.5}$), (2) if any carbonate buffering occurred ([Ca] + [Mg] > 0.7 mmol/L), (3) if acidification occurred (TIC < 1.4 mmol/L due to acid titration), and (4) if the supernatant was supersaturated for CO_2 with respect to atmosphere in the head-space. It can be seen that most supernatants were close to carbonate equilibrium with atmospheric CO_2 pressure (Table 7), but several samples had a TIC of zero indicating (the onset of) acidification. Only a small number of samples have supernatants with strong CO_2 supersaturation. Fig. 4b

Table 7
Selected supernatant parameters and SI's

Sample (–)	Facies	Al (μmol/L)	Fe (μmol/L)	Si (mmol/L)	SO_4 (mmol/L)	TIC (mmol/L)	Ca + Mg (mmol/L)	pH (–)	pCO_2 (atm)	Calcite (SI)	Dolomite (SI)	Gypsum (SI)	Jarosite (SI)
C15	ChanOX	<0.1	1.4	0.19	0.1	2.6	1.6	7.1	−2.1	−0.6	−2.0	−2.1	
C23	ChanOX	<0.1	1.0	0.20	0.1	2.3	1.5	8.3	−3.2	0.5	0.2	−2.2	
C01	ChanRE	<0.1	0.6	0.11	3.3	1.4	3.9	8.1	−3.3	0.5	−0.1	−0.9	
P03	ChanRE	<0.1	0.7	0.06	1.5	1.5	2.2	8.0	−3.1	0.2	−0.7	−1.4	
P04	ChanRE	<0.1	0.4	0.07	1.3	1.3	2.5	7.9	−3.1	0.1	−0.9	−1.3	
P06	ChanRE	<0.1	5.0	0.16	1.5	1.3	2.2	7.6	−2.8	−0.3	−1.4	−1.4	
P08	ChanRE	<0.1	1.2	0.05	1.0	1.4	1.8	8.0	−3.2	0.1	−0.8	−1.5	
C10	CrlvOX	<0.1	0.4	0.08	1.3	1.2	2.8	8.0	−3.2	0.1	−0.6	−1.4	
C16	CrlvRE	<0.1	0.7	0.07	2.4	2.3	3.9	7.5	−2.5	0.0	−0.9	−1.0	
C17	CrlvRE	<0.1	0.6	0.18	3.3	0.0	2.9	5.2				−1.0	
C18	CrlvRE	<0.1	1.2	0.04	2.2	1.3	2.7	7.7	−2.9	−0.2	−1.3	−1.2	
C20	CrlvRE	<0.1	0.7	0.04	2.7	1.5	3.3	8.0	−3.1	0.3	−0.4	−1.0	
P10	DuneRE	34.9	10.4	0.56	0.3	0.1	0.8	4.5	−2.5	−6.6	−14.0	−2.1	0.5
P11	DuneRE	195.3	88.8	0.71	0.4	0.1	0.4	4.5	−2.8	−7.1	−14.8	−2.5	3.6
P12	DuneREca	<0.1	3.2	0.09	1.6	1.0	2.5	7.4	−2.7	−0.6	−2.1	−1.3	
C05	FlbasRE	<0.1	5.0	0.11	2.0	0.1	3.6	6.4	−3.1	−2.8	−6.4	−1.1	
C07	FlbasRE	7.1	5.3	0.09	3.3	0.2	3.2	5.9	−2.6	−3.4	−7.7	−1.0	2.1
C09	FlbasRE	<0.1	0.5	0.08	3.1	0.6	3.6	7.2	−2.8	−1.0	−2.9	−1.0	
C13	OrgRE	200.5	49.7	0.60	23.5	0.0	18.0	3.7				0.1	1.7
C22	OrgRE	1.5	1.2	0.28	12.5	0.0	11.3	5.6				−0.2	

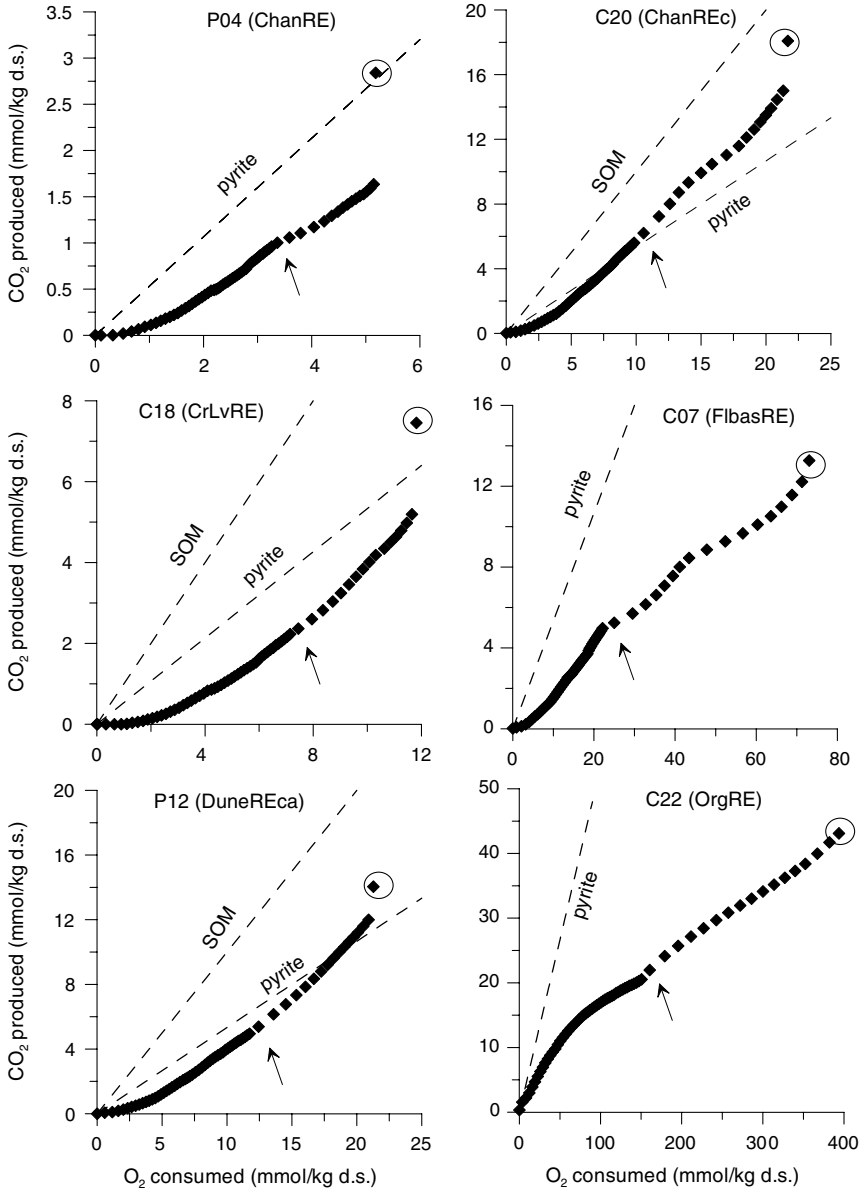

Fig. 2. CO_2 production vs. O_2 consumption for some representative samples showing changing CO_2/O_2 slopes over time. The dotted lines represent the CO_2/O_2 slopes for pyrite oxidation (8/15) and SOM (1/1) oxidation as indicated. Data points in circles represent the total CO_2 production including alkalinity in the supernatant at the end of the incubation. The arrow indicates where shaking rates increased from 100 rpm to 200 rpm.

shows the Ca+Mg concentration versus [SO_4], indicating whether pyrite oxidation was (1) unbuffered (reaction R1a, Table 2; area under dotted line in Fig. 4b), (2) buffered (reaction 1b, Table 2; dotted line in Fig. 4b), or (3) accompanied by CO_2-enhanced carbonate dissolution (reactions R1b plus 3, Table 2, area above dotted line in Fig. 4b). The off-set of the dotted line in Fig. 4b resembles the initial Ca + Mg concentration (0.7 mmol/L or half of the initial TIC concentration) due to CO_2-enhanced carbonate dissolution that occurred at the beginning of the experiments upon equilibration with atmospheric CO_2 pressure. It is clear that most supernatants plot on the dotted line reflecting buffered pyrite oxidation, but CO_2-enhanced carbonate dissolution occurred in a number of supernatants plot-

Table 8
Reaction rates at 100 rpm (1) and 200 rpm (2); the initial rates are also the maximum rates, the median rates represent steady-state rates, if applicable

Sample (–)	Facies	Initial rate (1 mmol $O_2 kg^{-1} d^{-1}$)	Median rate (1 mmol O_2 kg^{-1} d^{-1})	Initial rate (2 mmol O_2 kg^{-1} d^{-1})	Median rate (2 mmol O_2 kg^{-1} d^{-1})	[c]M2/M1 ratio
C15	ChanOX	0.017	0.011	0.040	0.025	2.4
C23	ChanOX	0.004	0.001	[a]N/A	[a]N/A	
C01	ChanRE	0.112	0.025	0.125	0.049	2.0
P03	ChanRE	0.078	0.018	0.051	0.039	2.1
P04	ChanRE	0.066	0.016	0.077	0.024	1.5
P06	ChanRE	0.157	0.032	0.114	0.063	2.0
P08	ChanRE	0.041	0.014	0.042	0.018	1.4
C10	CrlvOX	0.023	0.014	0.024	0.015	1.1
C16	CrlvRE	0.143	0.054	2.950	[b]0.449	8.3
C17	CrlvRE	0.230	0.058	2.474	[b]0.461	7.9
C18	CrlvRE	0.092	0.043	0.154	0.078	1.8
C20	CrlvRE	0.139	0.056	0.397	0.219	3.9
P10	DuneRE	0.028	0.011	0.019	0.008	0.7
P11	DuneRE	0.008	0.003	0.012	0.004	1.4
P12	DuneREca	0.233	0.071	0.374	0.146	2.1
C05	FlbasRE	0.706	0.156	3.093	[b]0.971	6.2
C07	FlbasRE	0.415	0.122	1.766	0.929	7.6
C09	FlbasRE	0.338	0.170	3.147	0.697	4.1
C13	OrgRE	3.697	1.940	25.630	10.355	5.3
C22	OrgRE	1.454	1.009	6.213	4.987	4.9

Rates were calculated from the O_2 consumption over 3 h intervals.
[a] Reactivity too low to calculate rate.
[b] No steady state rate reached after disturbance.
[c] Ratio of median rate 2 over median rate 1.

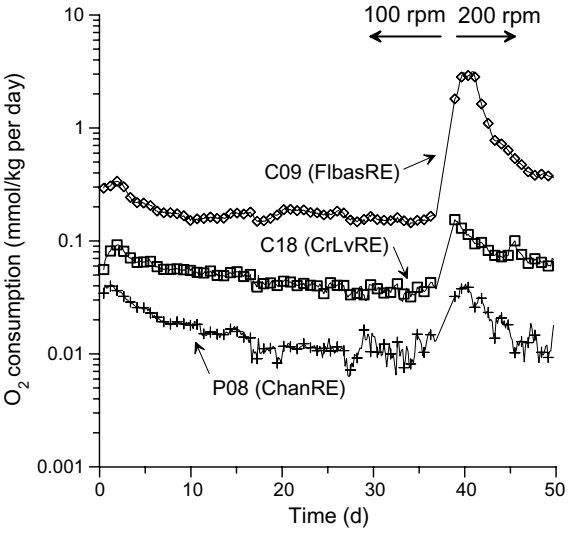

Fig. 3. Oxygen consumption rates based on 3-h measurement intervals vs. time. Examples for an anoxic channel sediment (P08), an anoxic crevasse–levee sediment (C18), and an anoxic flood basin sediment (C09).

ting above this line. These incubations have elevated CO_2 pressure in the supernatant indicating a non-equilibrium situation with the headspace. Acidified samples, (like C13 and C22 from the OrgRE facies, see inset), plot below the line, indicating H_2SO_4 production by unbuffered pyrite oxidation. Fig. 4c illustrates that carbonate dissolution was not the only source of CO_2 production, but that SOM oxidation contributed as well, as is implied by samples to the right of the line representing carbonate dissolution.

The absolute and relative MBC varied considerably among the incubations. In samples with alkaline supernatants and high TIC (Table 7), the relative MBC was always low (generally 1% of the PBC), indicating that little of the buffer capacity was used for neutralizing pyrite oxidation. In incubations with low overall reactivity (C15 and C23), a considerable part of the absolute MBC was needed to establish the carbonate-CO_2 equilibrium, leading to the absolute MBC exceeding the MRC_{Pyrite} by far. Supernatants with low alkalinity or low pH (C05, C07, C17, P10 and P11) had higher relative MBCs in the range of 2.4–15.1% of the PBC. Only two acidified incubations (C13 and C22, OrgRE facies) lost most of their PBC, and in C13 the MBC exceeded 100% of the PBC. Figure 6c shows that in the supernatants of C13 and C22 a significant part of the Ca + Mg can not be explained by carbonate dissolution alone, but excess Ca + Mg was desorbed from the exchange sites either due to acidification (protonation) or the loss of exchange sites with the oxidation of SOM. Exchange with other cations would not be likely because their relative low concentrations with respect to Ca+Mg, and the low pH which would favour protonation of the exchange sites. However, at pH < 4, an accessory source of Ca or Mg could be silicate dissolution. Thus, in acidified incubations like C13 and C22 Ca and Mg could have other sources apart from carbonate dissolution, thereby overestimating the MBC.

4. Discussion

4.1. Factors controlling potential reactivity

4.1.1. Facies approach

In this paper the facies approach is used to subdivide heterogeneous fluvio-eolian sediments into more homogeneous geogenic units. The results of the geochemical characterization show that each facies has unique reactive potentials. This suggests that a facies approach facilitates the characterization of the overall reactive properties of heterogeneous sediments, as has been suggested previously by others following a similar approach (Allen-King et al., 1998; Bersezio et al., 1999; Kleineidam et al., 1999). The facies model used here is universal for fluvial deposits (Miall, 1985, 1996) and defines lithological units at a scale that seems to be relevant for solute transport modelling (typically 10–100's of meters). In the case of the Rhine–Meuse deposits, intensive facies mapping of the region has already been done (Berendsen, 1986; Weerts, 1996). In addition, hydrologic and stochastic modeling was done by linking hydraulic conductivity to facies (Bierkens, 1994, 1996; Bierkens and Weerts, 1994; Weerts, 1996). Once the facies-distribution is well-known or could be modelled (see e.g. Deutsch and Tran, 2002; and references therein), facies will be of practical value in regionalizing reactive properties together with hydraulic properties for solute transport modeling at a field scale.

4.1.2. Effect of grain size

The observed differences in potential reactivity (PRC_{SOM}, PRC_{Pyr}, PBC) are partly related to grain size, because SOM and pyrite contents are usually enriched in fine grained sediments (Berner, 1971). The small grain size facies of the flood plains originated from low energy environments allowing organic matter particles to concentrate here rather

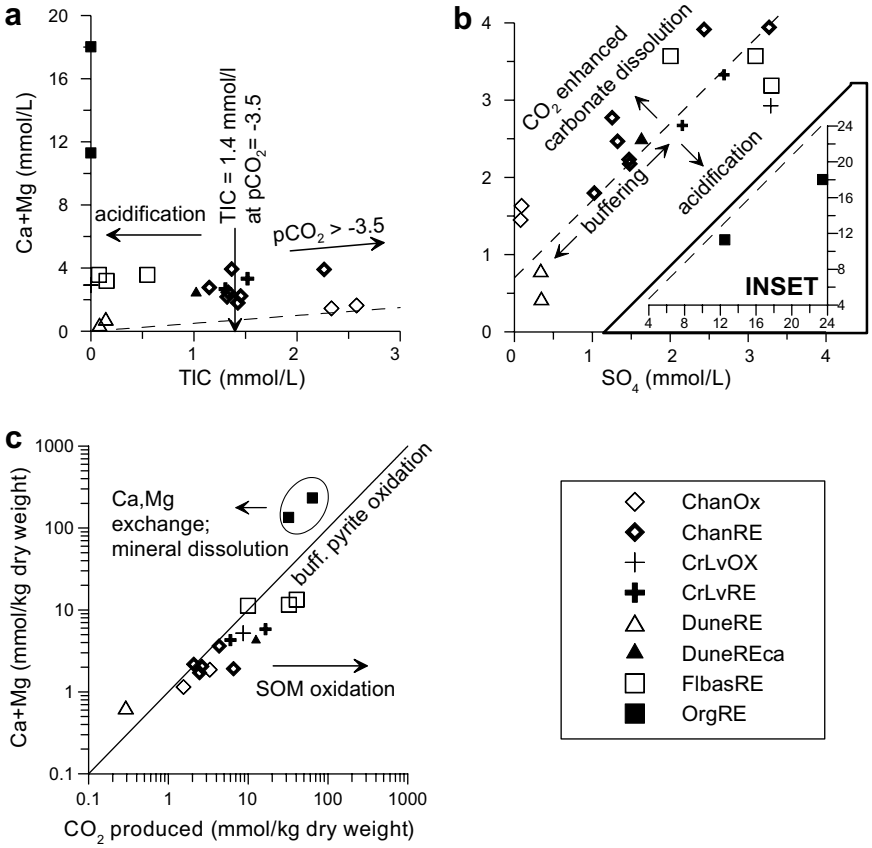

Fig. 4. Composition of the supernatants (see text for more explanation): (a) carbonate chemistry: dotted line represents theoretical ratio for $([Ca^{2+}]+[Mg^{2+}])/TIC$ in equilibration with atmospheric CO_2 pressure in the head-space; (b) $([Ca_{2+}]+[Mg_{2+}])/SO_4^{2-}$ ratios as indicator for operating buffering processes (carbonate dissolution, enhanced carbonate dissolution by increased CO_2 pressure in the supernatant, or no buffering at all). Inset shows peat samples with extreme SO_4^{2-} production; (c) the relative importance of pyrite oxidation and SOM oxidation.

than in the channel facies. In addition, the floodplains and crevasse-levee deposits formed a substratum for plant growth and peat formation, adding an authigenic source of SOM. Both the favourable settling environment and plant growth explain the high SOM contents in these facies.

It is generally known that anaerobic degradation of organic matter fuels pyrite formation via SO_4-reduction (Berner, 1972, 1984; Rickard, 1975), thus converting one reductant (SOM) into another (pyrite). Therefore, high pyrite contents are often associated with high SOM contents, as illustrated in Tables 3 and 4. The lower SOM contents in the sandy channel and dune facies thus result from an unfavourable settling environment and lack of post-depositional plant growth. For these reasons, these facies also have low pyrite contents. Additionally, the SOM in coarse-grained facies may be of low quality because of longer exposure to oxic water and intensive reworking before final burial (Hartog et al., 2004). Low quality SOM is less anaerobically degradable and subsequent pyritization is also less efficient.

van Helvoort et al. (2005) suggest a relation between carbonate content and grain size in fluvial deposits, because carbonate fragments originating from fresh water moluscs tend to be enriched in silty crevasse and levee deposits as a result of syn-depositional hydrodynamic sorting. This is reflected by predominantly high carbonate contents (PBC) in the CrlvOX and CrlvRE facies (Tables 3 and 4).

4.1.3. Effect of redox conditions

Tables 3 and 4 show that the prevailing redox condition is an important secondary factor determining the total potential reduction capacity.

Although not always true for the comparison of individual samples (Table 4), the median facies values (Table 3) yield higher PRCs for the reduced subfacies than for their oxidized counterparts. This indicates that the oxic subfacies must have lost part of their reduction capacities that were originally present, where PRC_{Pyrite} was preferentially lost over PRC_{SOM} in the oxic subfacies, as follows from higher PRC_{SOM}/PRC_{Pyrite} (Tables 3 and 4) ratios with respect to the anoxic subfacies. The oxic subfacies predominantly occur in the upper 1–1.5 m, where severe (recent) oxidation of the subsurface was caused by artificial drainage and subsequent lowering of the groundwater table. This has led to visible amounts of red Fe-hydroxide precipitates, and oxic groundwaters low in Fe and Mn (Table 5). Due to aerobic degradation, these facies are likely to contain more refractory SOM than their counterparts that are still anoxic. Note that for the channel facies the oxic and anoxic subfacies are quite similar, suggesting that syn-depositional aerobic degradation precluded preservation of PRC before post-depositional anoxic conditions prevailed. This explanation is supported by Hartog et al. (2004) who found low PRCs and MRCs in anoxic sandy riverine deposits that were intensively reworked before final burial.

The carbonate data in Table 3 shows that the oxic channel and crevasse-levee subfacies are slightly depleted of carbonate compared to their anoxic counterparts. This suggests that part of the carbonate has already dissolved by buffered pyrite oxidation. The oxic flood basin subfacies (FlbasOX), however, has higher carbonate contents than its anoxic counterpart (FlbasRE subfacies), because lime is locally applied on arable lands in the flood plains to restore soil quality after acidification. However, the FlbasRE subfacies and the OrgRE, which are considered as pristine deposits not artificially upgraded with carbonate supply, are prone to acidification because median PACs are close to or even exceed the buffering potential of carbonate (Tables 3 and 4). In anoxic environments, both the PRC_{tot} and PBC remain, showing the importance of anoxia in maintaining an overall high potential reactivity. In conclusion, the difference in reactive properties show that it makes sense to discriminate between oxic and anoxic subfacies within one main facies.

The imprint of palaeohydrologic conditions on potential reactivity is well illustrated by the high PRC_{tot} in the calcareous DuneREca subfacies as compared to the non-calcareous DuneRE subfacies. The inland dunes accumulated from wind-blown river-bed material in the Weichselian inter-glacial under dry and cold climate conditions. Although both subfacies have the same depositional history and are both anoxic at present, the DuneREca deposits are typically found at the base of dunes, currently at a depth greater than 5 m. The deeper parts of the inland dunes were flooded and buried soon after deposition due to the regional groundwater table rise during the Late Pleistocene and Early Holocene (van de Plassche, 1980, 1981; van Dijk et al., 1991), leading to anoxia soon after deposition. From the Early Holocene onwards, the groundwater table kept rising but at a much slower rate, and the upper parts of the dune deposits remained oxic and exposed until final burial in the Late Holocene. The small amount of PRC_{tot} left in the DuneRE subfacies indicates that much of the SOM was oxidized, and most of the carbonate was leached by infiltrating precipitation. Thus, a different post-depositional hydrological regime is the major cause of the low potential reactivity of the DuneRE when compared with the DuneREca facies.

The discussion above indicates that syn-depositional sorting (grain size), post-depositional redox conditions, and hydrological regime are interlinked factors controlling the preservation of potential reactivity. Because these factors will be much more similar within facies than between facies, sedimentary facies again appear to be an appropriate scale for the characterization of reactive properties of heterogeneous deposits.

4.2. Factors controlling measured reactivity

4.2.1. Overall measured reactivity and the effect of grain size

The high measured reduction capacities (MRC_{tot}) and the faster reaction rates in fine grained facies (Table 8) suggest an inverse relation between overall reactivity and grain size. Although a general particle size effect on reactivity is often found because specific surface increases (Bierens de Haan, 1991; Hartog et al., 2002, 2004), one may wonder whether this holds for pyrite and SOM as reductants. Pyrite particles typically occur as framboids or other small particles having their own characteristic surface morphology and kinetic characteristics. SOM may occur as particles but it is frequently associated with charged solids in a sorbed manner (Kaiser and Guggenberger, 2000;

Soolins et al., 1996), and then its grain size differs from the matrix. An inverse relation between overall reactivity and grain size may exist because finely grained sediments have low permeability and solute fluxes are generally smaller, hence potential reductants are better protected from oxidation than in coarse sediments. The general observation is a loss of reactivity with increased exposure to oxidants ('ageing'), but other factors affecting reactivity include the molecular structure and composition of SOM (Canfield, 1994; Hartog et al., 2004; Hulthe et al., 1998; Lehmann et al., 2002), physical inhibition by surface precipitates of Fe-hydroxides on pyrite (Anderson et al., 2001; Eggleston et al., 1996; Nicholson et al., 1990), and whether a chemical or biological reaction pathway is followed (Fuseler et al., 1996; Marchand and Silverstein, 2002; Schippers and Sand, 1999).

In all incubations, the steady state rates are 3–8 times slower than the initial rates (Table 8), clearly indicating that longer exposure to molecular O_2 has a decrementing effect on overall reactivity ('ageing' effect). Doubling stirring rates leads to increased rates in the second steady-state (Table 8). This effect is more pronounced in the fine facies (FlbasRE, CrlvRE, OrgRE facies), but there is no simple one to one relation with grain size. The results however indicate that physical limitations affect the measured reaction rates of the finely grained facies more than the coarse facies. The above findings will have consequences for the translation of lab-measured reactivity to the reactivity in the field situation (see Section 4.3).

4.2.2. SOM reactivity

Focussing on SOM, the reduced reactivity in coarse facies could be explained by several factors. First, the Holocene channel deposits and Late Pleistocene dune deposits were partly, if not largely, derived from reworked older Pleistocene materials, and thus will contain SOM older than the time of final burial. The decrementing effect of intense reworking and transportation on the reactivity of SOM has been found previously (Canuel and Martens, 1996; Hartog et al., 2004; Hulthe et al., 1998; Ransom et al., 1998), and is likely to have affected the reactivity of SOM in the sandy channel and dune deposits more than in the finer facies. Second, infiltration of groundwater containing oxidants such as O_2, NO_3 and SO_4 in channel and dune deposits caused aerobic SOM degradation, enriching refractory SOM while the labile fraction was degraded. By contrast, in the FlbasRE facies anoxic conditions may have been prevailing since deposition. Because anaerobic degradation of SOM is a much slower process than aerobic degradation of refractory SOM (Hulthe et al., 1998), this could well explain the high reactivity of SOM in clayey facies (Table 6). Therefore, it is argued that the source of SOM, its depositional history, and preservation potentials vary strongly with lithology and depositional environment, and that SOM reactivity relates strongly to sedimentary facies.

4.2.3. Reactivity of pyrite

The relative MRC_{Pyrite} (Table 6) shows that pyrite was preferentially oxidized over SOM in the incubation experiments and thus is more reactive to molecular O_2 on a molar basis. This is in line with high PRC_{SOM}/PRC_{Pyrite} ratios in the oxic subfacies when compared to anoxic subfacies (Tables 3 and 4), suggesting that pyrite was preferentially removed from these facies.

A decrease of reactivity with longer exposure to O_2 has often been found (Moses et al., 1987; Schippers and Jorgensen, 2002; Zhang and Evangelou, 1996) and possibly resulted from Fe hydroxide precipitation, which was visually observed in most incubations. The freshly precipitated Fe-hydroxides likely decreased surface reactivity of pyrite grains by surface coating. Under acidifying conditions, pyrite oxidation may have temporarily increased due to surface coating removal and increased Fe(II) concentrations, but with ongoing acidification ($pH < 4.5$) as in C13, pyrite oxidation will slow down again because at low pH, the oxidation of Fe(II) by O_2 is slow (McKibben and Barnes, 1986).

4.2.4. Reactivity of carbonates

In some incubations, as in C17 (Fig. 5), acidification had already started before the PBC was exhausted, illustrating that carbonate dissolution was blocked or inhibited. Here, unbuffered pyrite oxidation (low or no CO_2 production) and buffered pyrite oxidation (high CO_2 production) alternate, suggesting that carbonate dissolution was temporarily hindered by Fe hydroxide precipitation on the mineral surface. Carbonate cannot dissolve until the hydroxide surface coating is removed by increased acidity, leading to episodic carbonate buffering rather than a continuous process. Another cause for discontinuous carbonate buffering could be that the oxidation of large organic molecules produces smaller intermediate organic acids that may

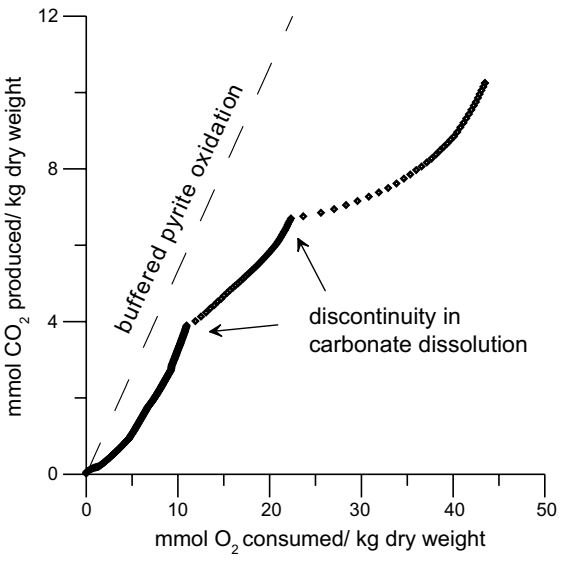

Fig. 5. Carbon dioxide production versus O_2 consumption of sample C17, implying discontinuous carbonate buffering. Dotted line represents CO_2/O_2 slopes for pyrite oxidation (8/15).

be reversibly sorbed on carbonates thereby inhibiting precipitation or dissolution of carbonates (Inskeep and Bloom, 1986). The recovery of CO_2 production in C17 after a period of acidification (Fig. 5) and the complete carbonate depletion in the acidified incubation C13 (pH 3.69) are in agreement with the reported rapid increase of carbonate dissolution rates under low pH conditions (Arvindson et al., 2003; De Giudici, 2002). The results show that acidification could start when the larger part of the PBC is still present. This means that in such a situation, facies may be prone to acidification even when their PBC exceeds the PAC.

4.3. Some implications for groundwater modelling

The results of this characterization study show that reactive properties vary widely with facies. This indicates that subsurface heterogeneity should be taken into account with groundwater quality modelling, and that the facies approach is a possible way forward. The facies classification system is universal for fluvial deposits (Miall, 1985, 1996) and could be applied in any other similar geological setting, provided there is enough geological data available. Facies seem to be the right scale of characterization, because larger discretizations will neglect heterogeneity, and smaller ones will be too complicated to trace and sample. The concept of potential reactivity characterization in terms of PRC, PBC and PAC seem useful internal parameters to quantify the potential resistance of groundwater systems to changing redox conditions and acidity. The potential reactivity parameters are easy to derive from cheap bulk chemical analysis and could be used for groundwater and soil vulnerability mapping (e.g. Morris et al., 2003) linking potential reactivity to oxidant and acidity loads by means of a mass balance. The results of this study do not show a simple relation between potential and measured reactivity, although finely-grained facies tend to have higher values for both. Without more specific information about local lithogenesis, it would be impossible to explain the measured reactivity from the potential reactivity.

The oxidation experiments always show high oxidation rates at first exposure to O_2, and a rapid drop in reactivity at (some degree of) steady state. In a field situation, the in-situ reactivity will decrease likewise with time. This suggests that short-term groundwater deterioration by subsurface oxidation is related to the availability and accessibility of fresh reactive sites (immediate oxidation at first exposure), and the long term effect will depend on steady-state reaction rates. It is noted here that the lab-measured reaction rates will certainly be higher than in-situ rates, because stirring dramatically enhances O_2 transfer to the reactive sites, either by enhanced gas exchange or by abrasion creating fresh reaction surfaces. In the field, however, oxidant supply depends on groundwater flow, hydraulic conductivity, and the contact surface between high and low conductivity facies (or facies distribution in the subsurface). The bottom line is that reactive transport models should include a relation between exposure time and reactivity in order to better predict short and long term effects of subsurface oxidation on groundwater quality.

In general, this study gives a new opportunity to couple reactivity and groundwater data to facies. As has been done for the hydraulic properties in the Rhine–Meuse delta (Bierkens, 1994, 1996; Bierkens et al., 2000), the data could be regionalized using indicator statistics and depositional models predicting the spatial facies distribution. This would be the next step in generating a reactive transport model for the specific case of the Rhine–Meuse deltaic plain. For similar geologic settings, the facies approach can be applied for sample classification and the potential reactivity can easily be derived from bulk chemical data. Although the measured reactivity data presented in this study could be

indicative for riverine deposits elsewhere, it ideally should be determined separately and interpreted with the local depositional history.

5. Conclusions

This characterization study shows that reactive properties vary widely with facies, and that a facies-based approach is a practical tool in characterizing reactivity of heterogeneous deposits. Both the potential reactivity and measured reactivity do not depend on grain size alone, but the syn/ post-depositional environment and ambient redox conditions are also important parameters. SOM was the main part of the potential reduction capacity, but pyrite measured reactivity is higher, as shown by relative depletion of pyrite in oxic subfacies and by the preferential oxidation in the incubations. Across facies, the measured reactivity of SOM and pyrite decreases with increased exposure to O_2. The oxidation experiments illustrate this by steady-state oxidation rates being much lower than rates measured at the initial exposure to molecular O_2. This implies that that reactive transport models should include a relation between exposure time and reactivity in order to predict short and long term effects of subsurface oxidation on groundwater quality.

References

Allen-King, R.M., Halket, R.M., Gaylord, D.R., Robin, M.J.L., 1998. Characterizing the heterogeneity and correlation of perchloroethene sorption and hydraulic conductivity using a facies-based approach. Water Resour. Res. 34, 385–396.

Anderson, M.S., Larsen, F., Postma, D., 2001. Pyrite oxidation in unsaturated aquifer sediments. reaction stoichiometry and rate of oxidation. Environ. Sci. Technol. 35, 4074–4079.

Arvindson, R.S., Ertan, I.E., Amonette, J.E., Luttige, A., 2003. Variation in calcite dissolution rates: a fundamental problem? Geochim. Cosmochim. Acta 67, 1623–1634.

Barber, L.B., Thurman, E.M., Runnells, D.D., 1992. Geochemical heterogeneity in a sand gravel aquifer: effect of sediment mineralogy and particle size on the sorption of chlorobenzenes. J. Contam. Hydrol. 9, 35–54.

Berendsen, H.J.A., 1986. Het landschap van de Bommelerwaard. Netherlands Geographical Studies, Utrecht University.

Berendsen, H.J.A., 1998. Birds-eye view of the Rhine–Meuse delta (The Netherlands). J. Coastal Res. 14, 740–752.

Berendsen, H.J.A., Stouthamer, E., 2001. Late Weichselian and Holocene palaeogeography of the Rhine–Meuse delta, The Netherlands. Palaeogeog. Palaeoclimatol. Palaeoecol. 161, 311–335.

Berendsen, H.J.A., Hoek, W.Z., Schorn, E., 1995. Late Weichselian and Holocene river channel changes of the rivers Rhine and Meuse in the central Netherlands (Land van Maas en Waal). In: Frenzel, B. (Ed.), ESF Project European Paleoclimatic Research, Special Issue. Verlag, pp. 151–171.

Berner, R.A., 1971. Principles of Chemical Sedimentology. McGraw-Hill, New York.

Berner, R.A., 1972. Sedimentary pyrite formation. Am. J. Sci. 268, 1–23.

Berner, R.A., 1984. Sedimentary pyrite formation; an update. Geochim Cosmochim. Acta 48, 605–615.

Bersezio, R., Bini, A., Giudici, M., 1999. Effects of sedimentary heterogeneity on groundwater flow in a Quarternary proglacial delta environment: joining facies analysis and numerical modelling. Sed. Geol. 129, 327–344.

Bierens de Haan, S., 1991. A review of the rate of pyrite oxidation in aqueous systems at low temperature. Earth-Sci. Rev. 31, 1–10.

Bierens de Haan, S., Rae, J.E., Parker, A., 1994. Pyrite oxidation in the tertiary sands of the London Basin aquifer. Appl. Geochem. 9, 161–173.

Bierkens, M.F.P., 1994. Complex confining layers. A stochastic analysis of hydraulic properties at various scales. Netherlands Geographical Studies, Utrecht University.

Bierkens, M.F.P., 1996. Modeling hydraulic conductivity of a complex confining layer at various spatial scales. Water Resour. Res. 32, 2369–2382.

Bierkens, M.F.P., Weerts, H.J.T., 1994. Application of indicator simulation to modeling the lithological properties of a complex confining layer. Geoderma 62, 265–284.

Bierkens, M.F.P., Finke, P.A., De Willigen, P., 2000. Upscaling and downscaling methods for environmental research. Kluwer Acxademic Publishers, Alterra, Wageningen University and Research Centre.

Bourg, A.C.M., Bertin, C., 1993. Biochemical processes during the infiltration of river water into an alluvial aquifer. Environ. Sci. Technol. 27, 661–666.

Canfield, D.E., 1994. Factors influencing organic carbon preservation in marine sediments. Chem. Geol. 114, 315–329.

Canuel, E.A., Martens, C.S., 1996. Reactivity of recently deposited organic matter: degradation of lipid compounds near the sediment–water interface. Geochim. Cosmochim. Acta 60, 1793–1806.

Christensen, T.H., Bjerg, P.L., Banwart, S.A., Jakobsen, R., Heron, G., Albrechtsen, H.J., 2000. Characterization of redox conditions in groundwater contaminant plumes. J. Contam. Hydrol. 45, 165–241.

Christiansen, J., Engesgaard, P., Bjerg, P.L., 1998. A physically and chemically heterogenous aquifer: field study and reactive transport modelling. Proceedings of GQ'98 Conference at Tuebingen, Germany. IAHS publication, pp. 329–336.

Cohen, K.M., 2003. Differential Subsidence Within a Coastal Prism: Late-Glacial-Holocene Tectonics in The Rhine–Meuse Delta, the Netherlands. PhD thesis, Utrecht University.

Davis, J.A., Fuller, C.C., Coston, J.A., Hess, K.M., Dixon, E., 1993. Spatial heterogeneity of geochemical and hydrologic parameters affecting metal transport in ground water. In: EPA Environmental research brief. EPA Environmental brief, pp. 1–22.

De Giudici, G., 2002. Surface control vs. diffusion control during calcite dissolution: Dependence of step-edge velocity upon solution pH. Am. Mineral. 87, 1279–1285.

Deutsch, C.V., Tran, T.T., 2002. FLUVSIM: a program for object-based stochastic modeling of fluvial depositional systems. Comput. Geosci. 28, 525–535.

Doussan, C., Poitevin, G., Ledoux, E., Detay, M., 1997. River bank filtration: modelling of the changes in water chemistry with emphasis on nitrogen species. J. Contam. Hydrol. 25, 129–156.

Eggleston, C.M., Ehrhardt, J.J., Stumm, W., 1996. Surface structural controls on pyrite oxidation kinetics: an XPS-UPS, STM, and modeling study. Am. Mineral. 81, 1036–1056.

Engesgaard, P., Kipp, K.L., 1992. A geochemical transport model for redox-controlled movement of mineral fronts in groundwater flow systems; a case of nitrate removal by oxidation of pyrite. Water Resour. Res. 28, 2829–2843.

Fuseler, K., Krekeler, D., Sydow, U., Cypionka, H., 1996. A common pathway of sulfide oxidation by sulfate reducing bacteria. FEMS Microbiol. Lett. 144, 129–134.

Gäbler, H.E., 1997. Mobility of heavy metals as a function of pH of samples from an overbank sediment profile contaminated by mining activities. J. Geochem. Explor. 58, 185–194.

Hartog, N., Griffioen, J., van der Weijden, C.H., 2002. Distribution and reactivity of O_2-reducing components in sediments from a layered aquifer. Environ. Sci. Technol. 36, 2338–2344.

Hartog, N., van Bergen, P.F., de Leeuw, J.W., Griffioen, J., 2004. Reactivity of organic matter in aquifer sediments: geological and geochemical controls. Geochim. Cosmochim. Acta 68, 1281–1292.

Hartog, N., van Bergen, P.F., Griffioen, J., 2005. Depositional and paleohydrogeological controls on the distribution of organic matter and other reactive reductants in aquifer sediments. Chem. Geol. 216, 113–131.

Hashagen, U., Jaekel, U., Schwartze, H., Vereecken, H., 1998. A physically and chemically heterogeneous aquifer: field study and reactive transport modelling. In: Herbert, M., Kovar, K. (Eds.), Groundwater Quality: Remediation and Protection. IAHS, pp. 337–342.

Heron, G., Christensen, T.H., 1994. The role of aquifer sediment in controlling redox conditions in polluted groundwater. In: Dracos, T., Stauffer, F. (Eds.), Transport and Reactive Processes in Aquifers. Balkema, Rotterdam, pp. 73–77.

Heron, G., Christensen, T.H., 1995. Impact of sediment-bound iron on redox buffering in a landfill leachate polluted aquifer (Vejen, Denmark). Environ. Sci. Technol. 29, 187–192.

Hesse, P.R., 1971. Cation and anion exchange properties, A Textbook of Soil Chemical Analyses. John Murray, London, pp. 88–105.

Huisman, D.J., Kiden, P., 1998. A geochemical record of Late Cenozoic sedimentation history in the soutern Netherlands. Geologie en Mijnbouw 76, 277–292.

Hulthe, G., Hulth, S., Hall, P.O.J., 1998. Effect of oxygen on degradation rate of refractory and labile organic matter in continental margin sediments. Geochim. Cosmochim. Acta 62, 1319–1328.

Inskeep, W.P., Bloom, P.R., 1986. Kinetics of calcite precipitation in the presence of water-soluble organic ligands. Soil Sci. Soc. Am. J. 50, 1167–1172.

Kaiser, K., Guggenberger, G., 2000. The role of DOM sorption to mineral surfaces in the preservation of organic matter in soils. Org. Geochem. 31, 711–725.

Kelly, W.R., 1997. Heterogeneities in ground-water geochemistry in a sand aquifer beneath an irrigated field. J. Hydrol. 198, 154–176.

Kinniburgh, D.G., Gale, I.N., Smedley, P.L., Darling, W.G., West, J.M., Aldous, P.J., O'Shea, M.J., 1994. The effects of historic abstraction of groundwater from the London Basin aquifers on groundwater quality. Appl. Geochem. 9, 175–195.

Kleineidam, S., Rügner, H., Grathwohl, P., 1999. Influence of petrographic composition/organic matter distribution of fluvial aquifer sediments on the sorption of hydrophobic contaminants. Sed. Geol. 129, 311–325.

Kölle, W., Strebel, O., Bötcher, J., 1985. Formation of sufate by microbial denitrification in a reducing aquifer. Water Supply 3, 35–40.

Korom, S.F., 1992. Natural denitrification in the saturated zone: a review. Water Resour. Res. 28, 1657–1668.

Larsen, F., Postma, D., 1997. Nickel mobilization in a groundwater well field: release by pyrite oxidation and desorption from manganese oxides. Environ. Sci. Technol. 31, 2589–2595.

Lehmann, M.F., Bernasconi, S.M., Barbieri, A., McKenzie, J.A., 2002. Preservation of organic matter and alteration of its carbon and nitrogen isotope composition during simulated and in situ early sedimentary diagenesis. Geochim. Cosmochim. Acta 66, 3573–3584.

MacIntyre, W.G., Antworth, C.P., Stauffer, T.B., Young, R.G., 1998. Heterogeneity of sorption and transport-related properties in a sand-gravel aquifer at Columbus, Mississippi. J. Contam. Hydrol. 31, 257–274.

Marchand, E.A., Silverstein, J., 2002. Influence of heterothrophic microbial growth on biological oxidation of pyrite. Environ. Sci. Technol. 36, 5483–5490.

Massmann, G., Tichomirowa, M., Merz, C., Pekdeger, A., 2003. Sulfide oxidation and sulfate reduction in a shallow groundwater system (Oderbruch Aquifer, Germany). J. Hydrol. 278, 231–243.

Massmann, G., Pekdeger, A., Merz, C., 2004. Redox processes in the Oderbruch polder groundwater flow system in Germany. Appl. Geochem. 19, 863–886.

McKibben, M.A., Barnes, H.L., 1986. Oxidation of pyrite in low temperature acidic solutions: Rate laws and surface textures. Geochim. Cosmochim. Acta 50, 1509–1520.

Miall, A.D., 1985. Architectural-elements analysis: A new method of facies analysis applied to fluvial deposits. Earth-Sci. Rev. 22, 261–308.

Miall, A.D., 1996. The Geology of Fluvial Deposits. Springer-Verlag, Heidelberg.

Mol, G., 2002. Soil acidification monitoring in the Netherlands. PhD. thesis University of Utrecht.

Morris, B.L., Lawrence, A.R.L., Chilton, P.J.C., Adams, B., C., C.R., Klinck, B.A., 2003. Groundwater and its susceptibility to degradation: A global assessment of the problem and options for management. In: Early Warning and Assessment Report Series, RS. 03-3, United Nations Environment Programme, Nairobi, Kenya.

Moses, C.O., Nordstrom, D.K., Herman, J.S., Mills, A.L., 1987. Aqueous pyrite oxidation by dissolved oxygen and ferric iron. Geochim. Cosmochim. Acta 51, 1561–1571.

Nicholson, R.V., Gillham, R.W., Reardon, E.J., 1990. Pyrite oxidation in carbonate-buffered solution. 2: Rate control by oxide coatings. Geochim. Cosmochim. Acta 54, 395–402.

Parkhurst, D.L., Appelo, C.A.J., 1999. User's guide to PHREEQC (version 2) – a computer program for speciation, reaction-path, 1D-transport, and inverse geochemical calculations. US Geol. Surv. Water Resour. Inv. Rep. pp. 99–4259.

Postma, D., Boesen, C., Kristiansen, H., Larsen, F., 1991. Nitrate reduction in an unconfined sandy aquifer: Water chemistry,

reduction processes, and geochemical modeling. Water Resour. Res. 27, 2027–2045.
Ransom, B., Kim, D., Kastner, M., Wainwright, S., 1998. Organic matter preservation on continental slopes: Importance of mineralogy and surface area. Geochim. Cosmochim. Acta 62, 1329–1345.
Rickard, D.T., 1975. The kinetics and mechanisms of pyrite formation at low temperatures. Am. J. Sci. 275, 636–652.
Ritsema, C.J., Groenenberg, J.E., 1993. Pyrite oxidation, carbonate weathering, and gypsum formation in a drained potential acid sulfate soil. Soil Sci. Soc. Am. J. 57, 968–976.
Santos, A., Alonso, E., Callejon, M., Jimenez, J.C., 2002. Heavy metal content and speciation in groundwater of the Guadiamar river basin. Chemosphere 48, 279–285.
Schipper, P.N.A.M., Appelo, C.A.J., van Helvoort, P.J., Broers, H.P., 2000. Zware metalen in het grondwater: pyrietoxidatie en desorptie (2). Resultaten geochemisch modelonderzoek Oostrum. H2O 33, 19–22.
Schippers, A., Jorgensen, B.B., 2002. Biogeochemistry of pyrite and iron sulfide oxidation in marine sediments. Geochim. Cosmochim. Acta 66, 85–92.
Schippers, A., Sand, W., 1999. Bacterial leaching of metal sulfides proceeds by two indirect mechanisms via thiosulfate or via plysulfides and sulfur. Appl. Environ. Microbiol. 65, 319–321.
Soolins, P., Homann, P., Caldwell, B.A., 1996. Stabilization and destabilisation of soil organic matter: mechanisms and controls. Geoderma 74, 65–105.
Stouthamer, E., Berendsen, H.J.A., 2000. Factors controlling the Holocene avulsion history of the Rhine–Meuse delta (The Netherlands). J. Sed. Res. 70, 1051–1064.
Stuyfzand, P.J., 1989. Hydrology and water quality aspects of Rhine bank groundwater in The Netherlands. J. Hydrol. 106, 341–363.
Stuyfzand, P.J., Griffioen, J., Broers, H.P., 1997. Chemisch onderzoek aan grondmonsters uit waterwingebieden: over het waarom, hoe en de toekomst. H2O 30, 9–13.
Törnqvist, T.E., 1993. Holocene alteration of meandering and anastomosing fluvial systems in the Rhine–Meuse delta (central Netherlands) controlled by sea-level rise and subsoil erodibility. J. Sed. Petrol. 63, 683–693.
Törnqvist, T.E., 1994. Middle and late Holocene avulsion history of the River Rhine (Rhine–Meuse delta, Netherlands). Geology 22, 711–714.
van Beek, C.G.E.M., 2000. Redox processes active in denitrification. In: Schüring, J., Schulz, H.D., Fischer, W.R., Bötcher, J., Duijnisveld, W.H.M. (Eds.), Redox Fundamentals, Processes and Applications. Springer, Berlin, pp. 152–160.
van Beek, C.G.E.M., Boukes, H., van Rijsbergen, D., Straatman, R., 1988. The threat of the Netherlands waterworks by nitrate in the abstracted ground water, as demonstrated on the well field Vierlingsbeek. Water Supply 6, 313–318.
van de Plassche, O., 1980. Holocene water-level changes in the Rhine–Meuse delta as a function of changes in relative sea level, local tidal range and river gadient. Geologie en Mijnbouw 59, 343–351.
van de Plassche, O., 1981. Sea-level, groundwater and basal peat growth – a reassessment of data from The Netherlands. Geologie en Mijnbouw 60, 401–409.
van Dijk, G.J., Berendsen, H.J.A., Roeleveld, W., 1991. Holocene water level development in The Netherlands' river area; implications for sea-level reconstruction. Geologie en Mijnbouw 70, 311–326.
van Helvoort, P.J., 2003. Complex Confining Layers. A Physical and Geochemical Characterization of Heterogeneous Unconsolidated Fluvial Deposits Using a Facies-based Approach. PhD. thesis, Utrecht University.
van Helvoort, P.J., Broers, H.P., Schipper, P.N.A.M., Appelo, C.A.J., 2000. Zware metalen in het grondwater: pyrietoxidatie en desorptie (1). H2O 33, 15–18.
van Helvoort, P.J., Filzmoser, P., van Gaans, P.F.M., 2005. Sequential factor analysis as a new approach to multivariate analysis of heterogeneous geochemical datasets: an application to a bulk chemical characterization of fluvial deposits (Rhine–Meuse delta, The Netherlands). Appl. Geochem. 20, 2233–2251.
von Gunten, H.R., Karametaxas, G., Krähenbühl, U., Kuslys, M., Giovanolly, R., Hoehn, E., Keil, R., 1991. Seasonal biogeochemical cycles in riverborne groundwater. Geochim. Cosmochim. Acta 55, 3597–3609.
Weerts, H.J.T., 1996. Complex Confining Layers. Architecture and hydraulic properties of Holocene and Late Wechselian deposits in the fluvial Rhine–Meuse delta. Netherlands Geographical Studies, Utrecht University, The Netherlands.
Weerts, H.J.T., Berendsen, H.J.A., 1995. Late Weichsilian and Holocene fluvial paleogeography of the southern Rhine–Meuse delta (the Netherlands). Geologie en Mijnbouw 74, 199–212.
Zhang, Y.L., Evangelou, V.P., 1996. Influence of iron oxide forming conditions on pyrite oxidation. Soil Sci. 161, 852–864.
Zhu, C., Burden, D.S., 2001. Mineralogical compositions of aquifer matrix as necessary initial conditions in reactive contaminant transport models. J. Contam. Hydrol. 51, 145–161.